

PHOTON AND DI-PHOTON PRODUCTION AT ATLAS

Marco Delmastro^{a b}
CERN^c

Abstract. The latest ATLAS measurements of the cross section for the inclusive production of isolated prompt photons in pp collisions at a centre-of-mass energy $\sqrt{s} = 7$ TeV at the LHC are presented, as well as the measurement of the di-photon production cross section.

1 Overview

The production of prompt photons at hadron colliders provides means for testing perturbative QCD predictions, providing a colorless probe of the hard scattering process. The dominant production mechanism of single photons in pp collisions at the Large Hadron Collider (LHC) energies is $qg \rightarrow q\gamma$, while the production of di-photon final states mainly occurs through quark-antiquark annihilation, $q\bar{q} \rightarrow \gamma\gamma$, and gluon-gluon interaction $gg \rightarrow \gamma\gamma$ mediated by a quark box diagram. In both single and di-photon final states, parton fragmentation to photon also contributes.

Because of the main production mechanism, the measurement of the inclusive photon cross section at the LHC can constrain the gluon density in protons. The study of the distribution of the azimuthal separation between the two photons in di-photon events can provide insight on the fragmentation model, while for balanced back-to-back di-photons the di-photon cross section is sensitive to soft gluon emission, which is not accurately described by fixed-order perturbation theory. Di-photon production is also an irreducible background for some new physics processes, such as the Higgs decay into photon pairs.

We present here two measurements of the inclusive isolated prompt photon production cross section as a function of the photon transverse energy E_T^γ , using pp collision data collected in 2010 with the ATLAS detector [4] at the LHC at a center-of-mass energy of 7 TeV. The former is based on an integrated luminosity $\int \mathcal{L} dt = (0.88 \pm 0.1) \text{ pb}^{-1}$ [1], and provides a measurement of the cross section for $15 \leq E_T^\gamma < 100$ GeV in the photon pseudorapidity η intervals $[0,0.6)$, $[0.6,1.37)$ and $[1.52,1.81)$. The latter uses the full 2010 data sample $\int \mathcal{L} dt = (36.4 \pm 1.2) \text{ pb}^{-1}$ [2], covering the $40 \leq E_T^\gamma < 400$ GeV E_T^γ range and extending to the $[1.81,2.37)$ pseudorapidity region.

We also present the measurement of the inclusive di-photon cross section as a function of the di-photon invariant mass $m_{\gamma\gamma}$, the di-photon system momentum $p_{T,\gamma\gamma}$ and the azimuthal separation between the two photons $\Delta\phi_{\gamma\gamma}$, using an integrated luminosity $\int \mathcal{L} dt = (36.0 \pm 0.1) \text{ pb}^{-1}$ [3].

^ae-mail: Marco.Delmastro@cern.ch

^bOn behalf of the ATLAS Collaboration

^cThe author is now at LAPP (IN2P3/CNRS, France).

2 Photon selection, reconstruction and identification in ATLAS

Single photon events are triggered in ATLAS using a high-level trigger with a nominal transverse energy threshold of 10 GeV [1] or 40 GeV [2]; di-photon events are triggered by two photon candidates having $E_T^\gamma > 15$ GeV [3]. Using unbiased or lower-threshold triggers, these triggers are found to be fully efficient for photons and di-photons passing the selection criteria of the analyses.

Photon candidates depositing their energy in the ATLAS Liquid Argon (LAr) electromagnetic calorimeter (EMC) in the regions $|\eta| < 1.37$ and $1.52 \leq |\eta| < 2.37$ are reconstructed. The photons converting in e^+e^- pairs before reaching the EMC (about 30% in the samples under study) are separated from electrons by associating the reconstructed tracks and conversion vertices to the EMC energy deposit. The overall photon reconstruction efficiency is about 85% (75%) for $|\eta| < 1.37$ ($1.52 \leq |\eta| < 2.37$), the main losses being due to non-operational LAr EMC readout modules during the 2010 data taking. In the inclusive photon analyses photon candidates are required to have reconstructed E_T^γ larger than 15 GeV [1] and 45 GeV [2]; in the di-photon measurement both photon candidates in a event must have $E_T^\gamma > 16$ GeV.

Background from non-prompt photons originating from decays of leading neutral mesons inside jets (e.g. π^0) is suppressed by means of selections on the electromagnetic shower momenta, and of a requirement on the photon isolation in the EMC. Photon candidates must pass tight identification criteria based on nine discriminating variables computed from the lateral and longitudinal profiles of the energy deposited in the EMC, and in the hadronic calorimeter behind it. The first LAr EMC layer is finely segmented such to allow the resolution of two maxima in the energy deposit, typical of the superposition of two photons from a neutral meson decay. The efficiency of these selections ranges from $\sim 60\%$ to $\sim 90\%$ for increasing E_T^γ .

The photon transverse isolation energy E_T^{iso} is computed from the sum of the energies in the LAr EMC cells in a cone of radius 0.4 in the $\eta - \phi$ plane around the photon candidate axis. The contribution to E_T^{iso} from the photon itself is subtracted, as well as the energy from the soft-jet activity from the underlying event and from event pileup [5]. All measurements presented here require $E_T^{\text{iso}} < 3$ GeV.

3 Background subtraction

After the selection criteria described above, a residual contribution of background candidates pollutes the photon and diphoton samples. In the inclusive photon analysis, this background contamination is estimated using a data-driven counting technique based on the observed number of events in the control regions (sidebands) of a two-dimensional plane formed by the photon transverse isolation energy and a photon identification variable. Corrections for signal

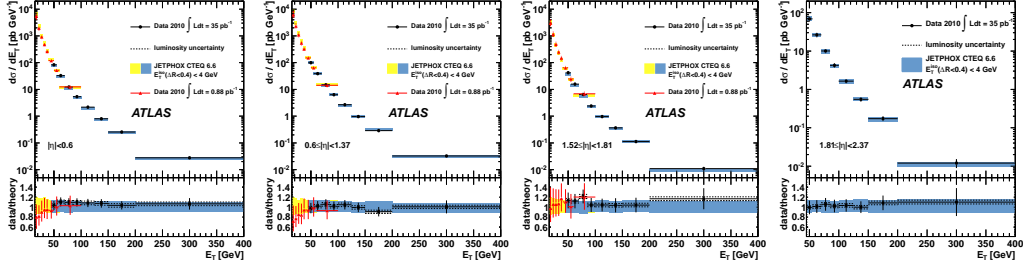


Figure 1: Measured cross section of isolated prompt-photon production as a function of E_T^γ in different pseudorapidity ranges, compared with theoretical predictions. The red triangle represent the results from [1], the black dots those from [2].

leakage in the background control regions and for correlation between the two variables in background events are taken into account.

The same sideband method is iterated on di-photon event on the leading and sub-leading photon candidates, allowing to separate the di-photon signal from the photon-jet and jet-jet background components. Alternatively, a matrix approach classifying the events in categories according to whether each of the tight photon candidates passes or not the isolation criteria, or a template approach fitting the distributions of the isolation energy profiles, are used and give compatible yield results.

In both inclusive and di-photon analyses the residual contamination from electron misidentified as photons is evaluated and subtracted.

4 Cross section measurements

Inclusive prompt photon and di-photon cross sections are respectively measured in different bins of E_T^γ and $m_{\gamma\gamma}, p_{T,\gamma\gamma}, \Delta\phi_{\gamma\gamma}$ from the extracted signal yields, the corresponding integrated luminosities, and the trigger, reconstruction and selection efficiencies. The measured cross sections are affected by different systematic uncertainties, primarily associated to the uncertainty on the photon reconstruction efficiency (3-4% due to the isolation efficiency cut, and 1-2.5% associated to the limited knowledge of the material upstream the EMC); to the uncertainty on the photon identification efficiency (ranging from 8% to 1.5%, the higher values being applicable at lower E_T^γ); to uncertainty on the signal yields due the background subtraction technique (at most 10%, mostly associated to the definition of the background control regions and the photon energy scale).

Figure 1 shows the inclusive photon cross sections as a function of E_T^γ in four different η regions. The theoretical pQCD cross sections, computed with a fixed-order NLO parton-level generator (JETPHOX [6]) for photons having

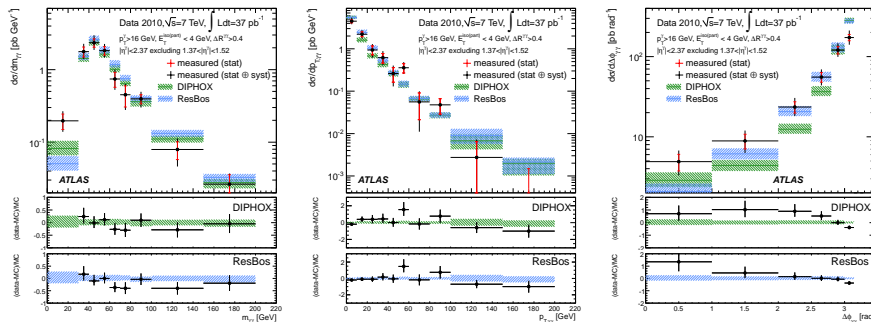


Figure 2: Measured cross section of isolated di-photon production as a function of $m_{\gamma\gamma}$, $p_{T,\gamma\gamma}$ and $\Delta\phi_{\gamma\gamma}$, compared with theoretical predictions.

parton transverse energy in a cone of radius 0.4 around the photon smaller than 4 GeV, are overlaid (yellow and blue bands, accounting for the scale and PDF uncertainties). The measured cross sections are in good agreement with the theoretical predictions for $E_T^\gamma > 35$ GeV, while at lower E_T^γ , where the contribution from parton-to-photon fragmentation is larger, the theory tends to overestimate the data, possibly hinting to the need of more accurate predictions.

Figure 2 shows the diphoton cross section as a function of $m_{\gamma\gamma}$, $p_{T,\gamma\gamma}$ and $\Delta\phi_{\gamma\gamma}$. Two theoretical predictions are overlaid for photons having parton transverse energy in a cone of radius 0.4 around the photon smaller than 4 GeV, one corresponding to a fixed-order NLO parton-level generator calculation (DIPHOX [7]), the other featuring transverse momentum resummation (RESBOS [8]). The agreement is generally good, but some deviations are observed for low $\Delta\phi_{\gamma\gamma}$ values, where both theoretical predictions underestimate the measurements. In this region the LO elements do not contribute to the cross section, and NLO is the first order giving non-zero contributions: more accurate NNLO predictions would provide clarifications on these residual discrepancies.

References

- [1] ATLAS, Phys. Rev. **D83** (2011) 052005 [arXiv:1012.4389].
- [2] ATLAS, submitted to Phys. Lett. B. [arXiv:1108.0253].
- [3] ATLAS, accepted for publication by Phys. Rev. D [arXiv:1107.0581].
- [4] ATLAS, JINST 3 (2008) S08003. ATLAS, [arXiv:0901.0512].
- [5] M. Cacciari, G.P. Salam and S. Sapeta, JHEP04, 065 (2010).
- [6] M. Fontannaz, J.P. Guillet and G. Heinrich, Eur. Phys. J. **C21** (2001) 303–312.
- [7] T. Binoth, J. P. Guillet, E. Pilon, M. Werlen, Eur. Phys. J. **C16** (2000) 311–330.
- [8] C. Balazs, E. L. Berger, P. M. Nadolsky, C. -P. Yuan, Phys. Rev. **D76** (2007) 013009.